3.6 Some Exploratory Tests

As will be described in the next chapter, under normal circumstances the AMR algorithm circumvents many numerical difficulties by simply preventing shock waves from crossing *fine-coarse* boundaries. Nevertheless, it is interesting to note the extent to which our *fine-coarse* boundary procedure can cope when it is forced to deal with a shock wave. To this end, we now present some results taken from a series of simple tests that essentially involved integrating the Euler equations using various different grid configurations. All these tests were performed using Roe's flux-difference splitting scheme in conjunction with the SUPERBEE limiter function.

The first set of results are taken from a test which computed the steady flow over a 10^o wedge for a free stream Mach number of 2. The solution to this problem consists of a single weak oblique shock which emanates from the tip of the wedge. The pressure and density ratios across this shock are 1.71 and 1.46 respectively, and the shock makes an angle of 29.3^o to the surface of the wedge. Figure 3.14 shows the resultant density contours for three different computational grids. Each contour plot contains thirty one contours drawn at 3.3% intervals of the density rise across the shock. To facilitate the interpretation of these contour plots, in figure 3.15 we present stereoscopic carpet plots for the density field. But note, so as to exaggerate the density rise $\rho_1 \rightarrow \rho_2$, these carpet plots show $\frac{(\rho - 0.75\rho_1)}{(\rho_1 - 0.75\rho_1)}$ and not $\frac{\rho}{\rho_1}$.

The top contour plot is a control which shows the quality of solution that can be expected from using a single uniform mesh. The flow solution is clearly monotone and yields both the correct shock angle and the correct shock jump. The bottom contour plot shows the AMR algorithm's preferred method of refinement, namely, to refine the whole length of a shock. Again the flow solution is clearly monotone. Now because the Euler equations contain no length scale, the thickness of the numerical shock profile will be self-similar with mesh spacing. So although the shock in the bottom contour plot appears thinner, it actually occupies the same number of cells as the shock in the top plot. Now, the most interesting case is shown by the middle contour plot. Here we have placed fine patches at three arbitrary positions along the length of the shock. Thus we have forced the *fine-coarse* boundary procedure to deal with a flow discontinuity. Pleasingly, the flow solution is almost monotone. Some small variations in the post-shock state can be observed from the carpet plot, but these must be less than 3% of the shock jump otherwise they would have appeared in the contour plot. Note the way that after the shock passes from a coarse part of the grid to a fine part of the grid it focuses down to its natural width on the fine mesh.

Another set of tests were performed which allowed arbitrary pre- and post-shock states to be specified across the bottom left-hand corner of the flow domain. Thus we could examine cases where a strong shock cuts across the computational grid at a respectable angle. Figure 3.16 shows density contours for the case where the shock angle is 32.6^o

to the horizontal, and the density and pressure rises across the shock are 5.1 and 33.7 respectively; the corresponding carpet plots are shown in figure 3.17. As before, the contour plots show thirty one contours drawn at 3.3% intervals of the density rise across the shock, and the carpet plots show $\frac{(\rho-0.75\rho_1)}{(\rho_1-0.75\rho_1)}$ rather than $\frac{\rho}{\rho_1}$. Even for this strong shock, tolerable results are obtained when the shock is allowed to pass through a *fine-coarse* boundary. However, when the shock wave is wholly encased within the fine mesh the flow solution is once again perfectly monotone.

Finally, we present two sets of results taken from a series of one-dimensional calculations that were performed so as to see what, if any, problems arose when a shock propagated across the boundary between two uniformly spaced meshes, one mesh being r times finer than the other. Specifically, we present the two possible cases, coarse to fine and fine to coarse, for a shock Mach number of 10 with a refinement ratio of 4. Figure 3.12 shows a sequence of density profiles which are taken at nominally uniform time intervals during the coarse to fine calculation. The calculation was started with the exact shock jump data, which was found using the moving shock relationships given in appendix A. As can be seen from this figure, two small disturbances appear soon after the calculation gets under way. These start up errors arise because once the exact shock position moves away from a cell interface, the projection of the true flow solution on to the discrete mesh will inevitably be slightly smeared. Thus the numerical scheme will no longer be presented with the exact shock data, and so both the $u_2 - a_2$ and u_2 characteristics will become activated, albeit at a very much reduced level compared to the u_s characteristic which carries the shock jump information. It should be noted, that these start up errors are not peculiar to Roe's scheme; for diffusive schemes such errors often become damped rather quickly and so evade detection. It has been argued that such errors are not generated continuously because the numerical shock settles down to a natural profile such that the phase errors between successive iterations, or those over a cycle of iterations, somehow cancel with one another. Interestingly, a similar set of perturbations is activated when the shock crosses into the fine mesh. For this case, these so-called spurious reflections are actually spurious tranmissions! We have managed to produce start up errors that are similar to these *fine-coarse* generated errors by simply connecting the pre- and post-shock states using linear ramp functions.[6] And, in general, the more cells between the two states the more pronounced the start up error. It is our contention that such errors are inevitable whenever the numerical shock profile is greatly perturbed from its natural profile, for today's so-called monotonicity preserving schemes are patently unable to guarantee the monotonicity of an arbitrary monotone profile separating a pair of states which satisfy the Rankine-Hugoniot relationships. But this is hardly surprising, for the model equations used to develop *shock-capturing schemes* cannot be expected to mimic all the subtleties of the Euler equations.

[6]For the linear advection equation, when a genuine discontinuity passes from a coarse to a fine mesh it is transformed into a linear ramp which stretches over $r-1$ mesh cells. The simplest way to prevent this from happening is to switch off the temporal interpolation along *fine-coarse* boundaries. Theoretically this switching could be done automatically using functions analogous to limiter functions.

Interestingly, as shown by figure 3.13, the results for the fine to coarse calculation are better behaved than those for the coarse to fine calculation. Indeed, now the *fine-coarse* generated errors are no larger than the start up errors. This is good news, for in the unlikely event that the AMR algorithm fails to stop a shock wave from crossing a *fine-coarse* boundary, in all probability the shock will be escaping from a fine mesh to a coarse mesh, and so little damage will occur.

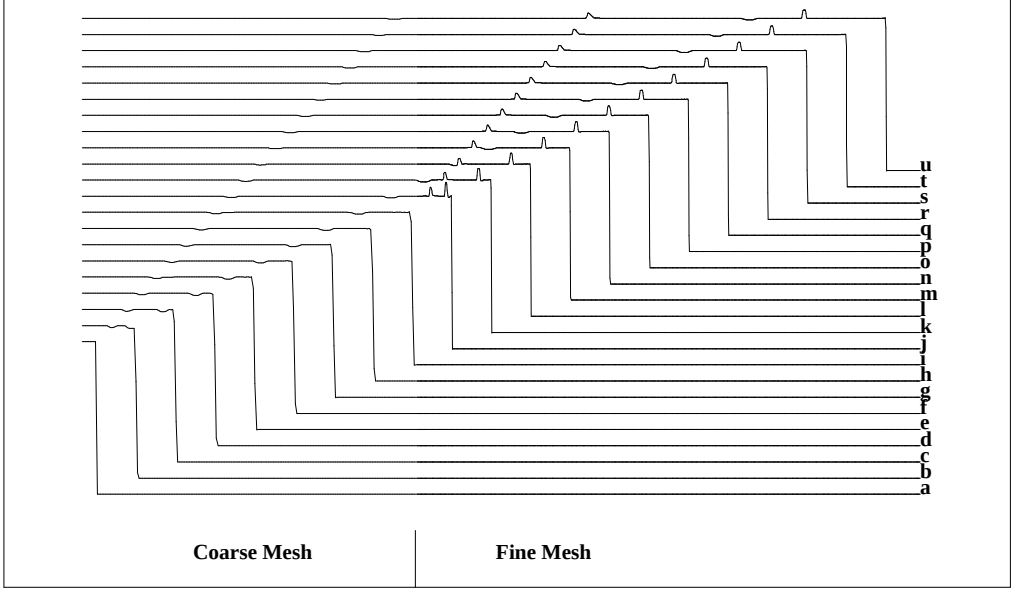

Figure 3.12: Propagation of a shock wave from a coarse mesh to a fine mesh

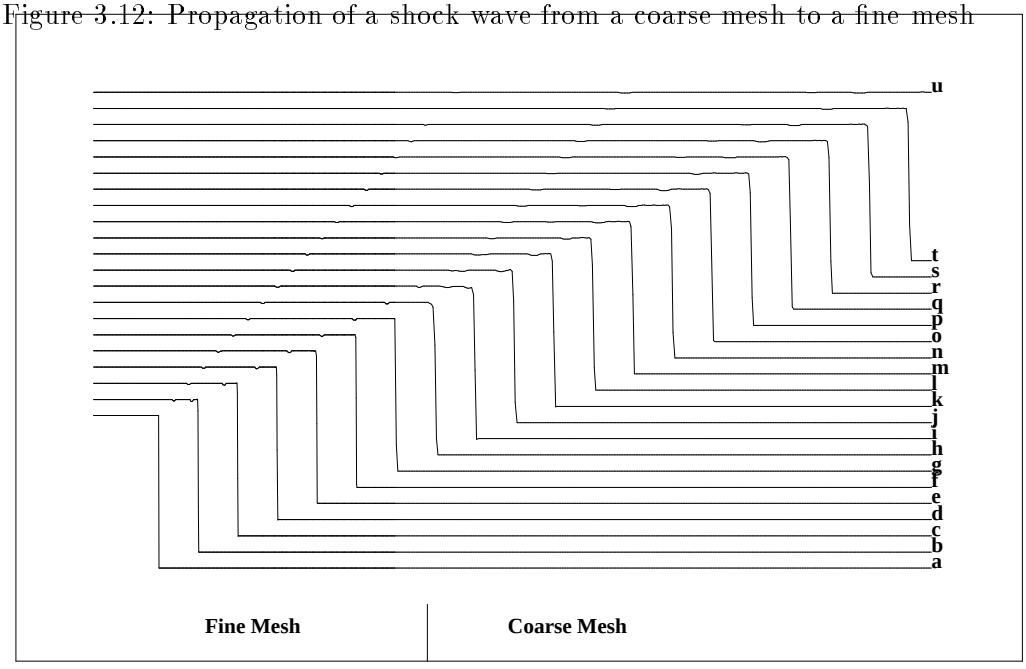

Figure 3.13: Propagation of a shock wave from a fine mesh to a coarse mesh

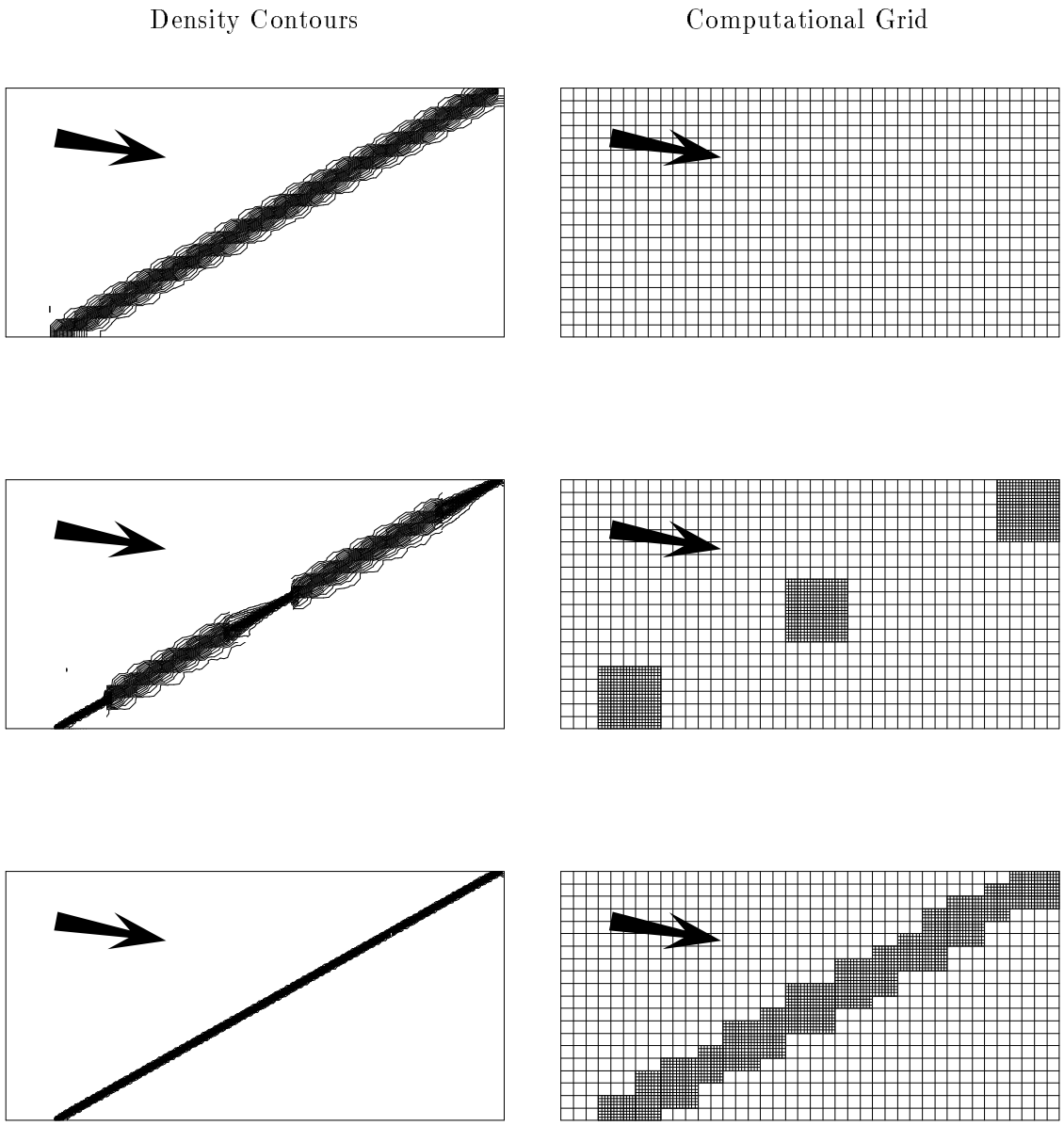

Figure 3.14: Exploratory tests for a weak oblique shock.

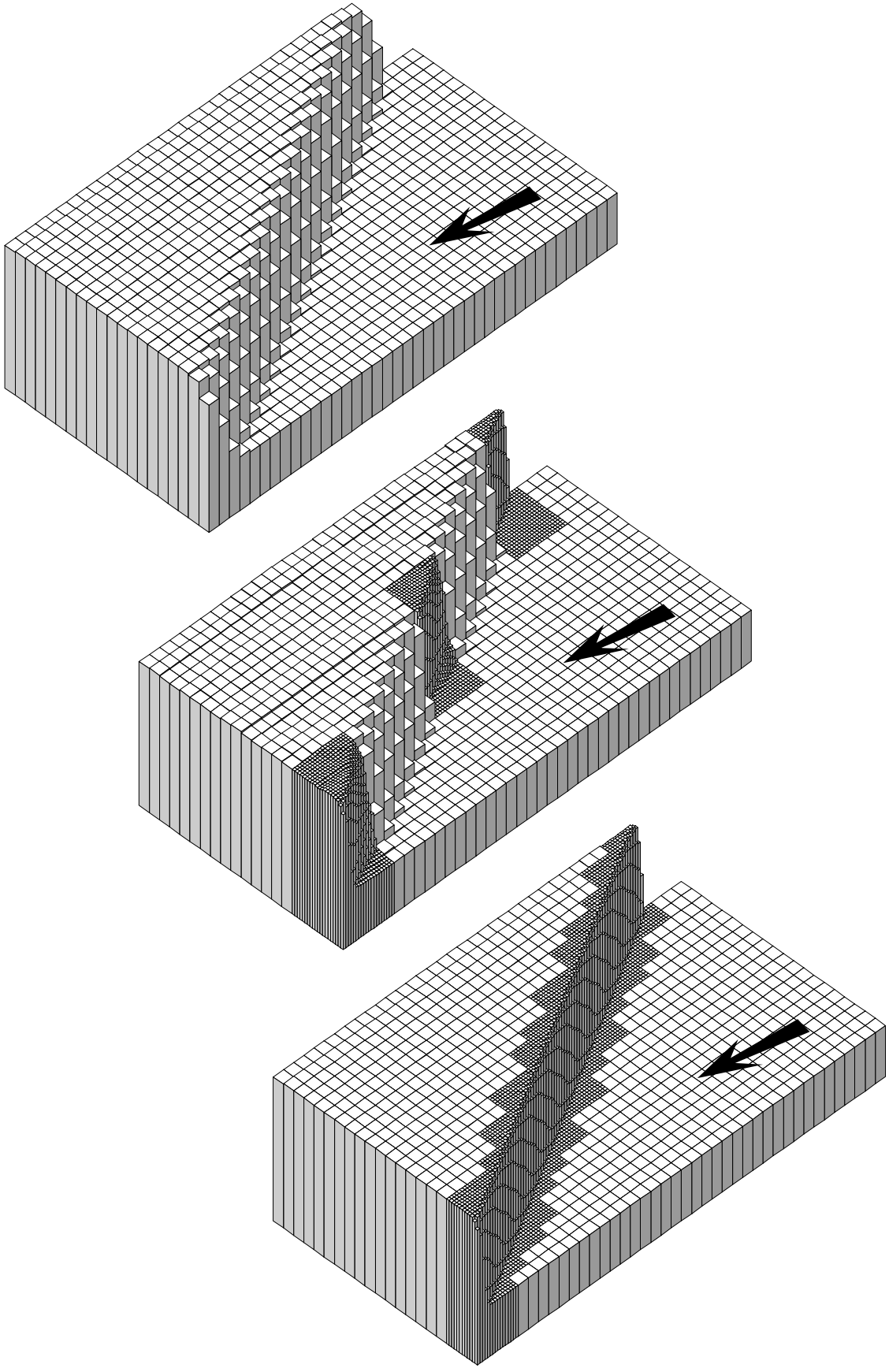

Figure 3.15: Carpet plots for the density contours shown in figure 3.14.

Density Contours

Computational Grid

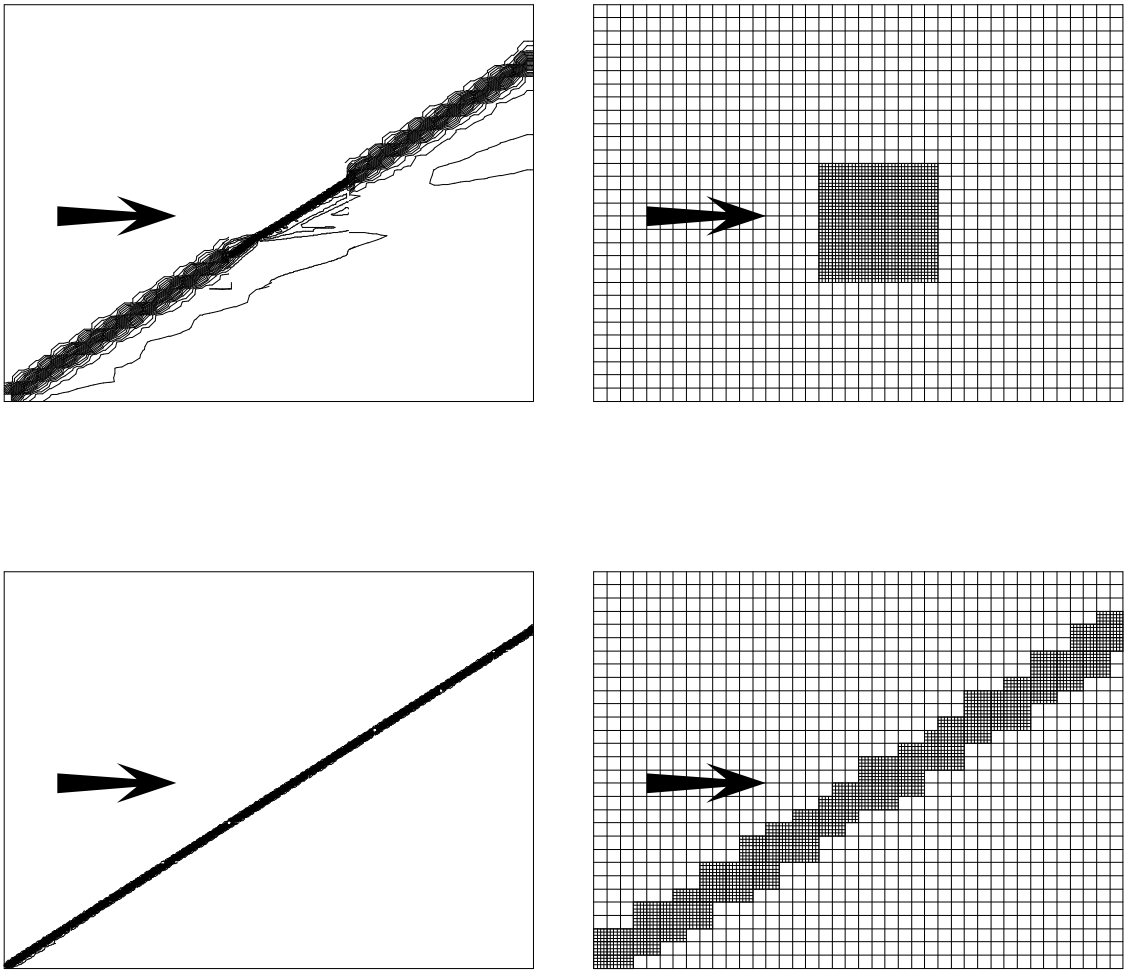

Figure 3.16: Exploratory tests for a strong oblique shock.

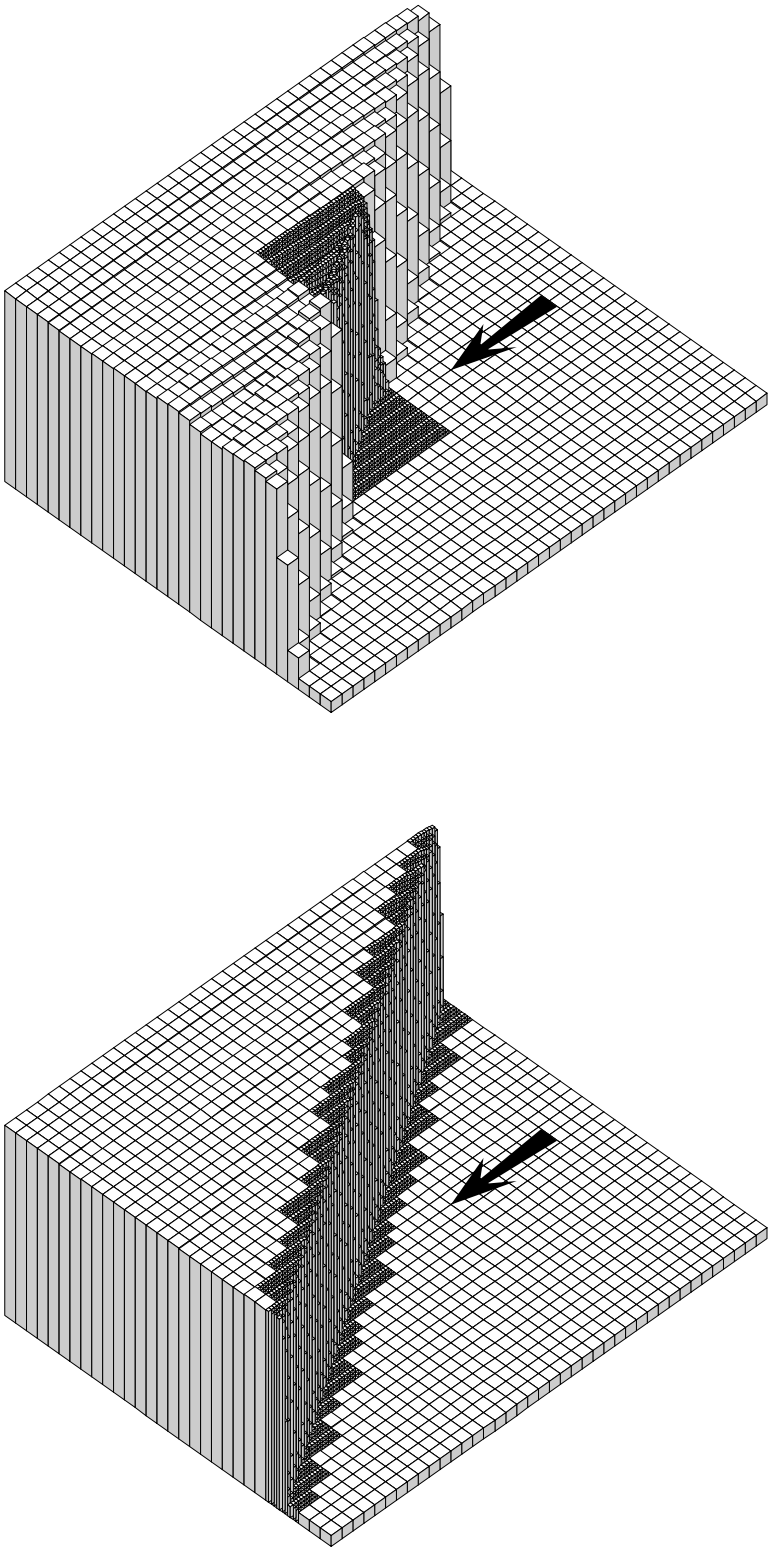

Figure 3.17: Carpet plots for the density contours shown in figure figure 3.16.

3.7 Closing Comment

A computational scheme such as the AMR algorithm contains many elements, and the success of the scheme depends on whether or not these elements are combined in a harmonious manner. So, although a particular element may have a number of defects when it is viewed in isolation, it does not necessarily follow that such defects are important. For example, it is clear that our treatment of *fine-coarse* boundaries is far from perfect. However, it has proved to be more than adequate for the role which it has been asked to play — if a defect can be circumvented, why worry about it? Indeed, if we had permitted ourselves the luxury of investigating, fully, every interesting byway that we have unearthed during the course of this study then the AMR algorithm would as yet be unfinished. At least we now have a platform upon which to build. Unfortunately our time has run out, leaving a number of areas where improvements could still be made. Nevertheless, as will be shown in chapter 6, the algorithm does not require radical surgery, but just some fine-tuning.